

Surface-induced Magnetism Fluctuations in Single Crystal of NiBi₃ Superconductor

Xiangde Zhu,^{1,*} Hechang Lei,² C. Petrovic,² and Yuheng Zhang¹
¹ *High Magnetic Laboratory, Chinese Academy of Sciences and University of Science and Technology of China, Hefei 230026, People's Republic of China*

² *Condensed Matter Physics and Materials Science Department, Brookhaven National Laboratory, Upton, New York 11973, USA*

(Dated: July 16, 2012)

We report anisotropy in superconducting and normal state of NiBi₃ single crystals with $T_c = 4.06$ K. The magnetoresistance results indicate the absence of scattering usually associated with ferromagnetic metals, suggesting the absence of bulk long range magnetic order below 300 K. However, the electron spin resonance results demonstrate that ferromagnetism fluctuations exist on the surface of the crystal below 150 K.

PACS numbers: 75.70.-i, 74.70.Ad, 76.30.-v

I. INTRODUCTION

Ferromagnetism (FM) and superconductivity (SC) are two fundamental condensed matter phenomena. The former one favors all spins parallel, while in the latter one carriers condense in Cooper pairs where spins are antiparallel in classical BCS scenario. The superconducting properties of ferromagnetic superconductors are currently under debate. The p -wave superconductivity was proposed to coexist with itinerant ferromagnetism.¹ So far, the coexistence of FM and SC has been discovered in UGe₂,² URhGe,³ and UCoGe.⁴ A binary intermetallic compound, ZrZn₂ was reported to exhibit coexistence of ferromagnetism and superconductivity.⁵ Interestingly, superconductivity originates from the surface alloy rich in Zn.⁶ In addition, the spin-singlet pairing superconductivity and magnetic order parameters entwine each other in a spatially modulated pattern, which allows for their mutual coexistence in for example borocarbides,⁷ CeCoIn₅ in high magnetic fields,^{8,9} HoMo₆S₈,¹⁰ P doped EuFe₂As₂,¹¹ and ErRh₄B₄.¹²

Ni-Bi based compounds show complex physics phenomena including antiferromagnetism and superconductivity. LaNiBiO is isostructural to $LnFeAsO$ (Ln represents the rare earth elements) iron based high temperature superconductors. CeNiBi₂ is an antiferromagnetic metal, whose structure is similar to that of iron based superconductors.¹³ Interestingly, when Ni deficient, CeNi_{1-x}Bi₂ shows superconductivity.¹³ Recently, NiBi₃, an intermetallic superconductor with $T_c = 4.06$ K, attracted some attention, due to possible coexistence of ferromagnetism (Curie temperature < 750 K) and superconductivity in polycrystals.¹⁴ Coexistence of ferromagnetism and superconductivity is also observed in nano structured crystals below 30 K.¹⁵ The polycrystal NiBi₃ is reported to have large field dependent thermal transport properties and magneto-resistance (MR).¹⁶ In addition, the magnetic ions doping of Co results in T_c enhancement and onset of resistivity drop around 10 K in NiBi₃.¹⁷ These results suggest that magnetic order is related to superconductivity in NiBi₃. However, other two groups reported that no magnetism was observed in

NiBi₃ bulk crystals.^{15,18} It should be noted that magnetic impurities cannot be avoided during synthesis process for nominal stoichiometric 1:3 composition according to the Ni-Bi phase diagram.¹⁹ Thus, it is necessary to investigate the magnetism of NiBi₃ in impurity-free single crystals. Here, we report the comprehensive study of NiBi₃. We show evidence of the ferromagnetism fluctuations induced at the surface below 160 K. No large MR or field dependant heat capacity is observed, which indicates that no bulk magnetism exists in NiBi₃.

II. EXPERIMENTAL

Single crystals of NiBi₃ were grown from self-flux method with Ni:Bi = 1:10 mol ratio. This method avoids the NiBi phase and other magnetic impurity in the solid state reaction with of stoichiometric Ni:Bi (1:3) according to the Ni-Bi phase diagram.²⁰ High purity Ni shot and Bi pieces were mixed and sealed in an evacuated quartz tube. The tube was heated to and soaked at 1150 °C for 2 hours, then cooled down to 400 °C with 5 °C/h. Finally, the tube was spun in a centrifuge to separate the Bi flux. As is shown in Fig. 1 (b), needle like, silver colored single crystals with size of $\sim 2 \text{ mm} \times 0.2 \text{ mm} \times 0.2 \text{ mm}$ (with b axis of the longest dimension) were obtained. The single X-ray data were collected using the Bruker APEX2 software package Apex2 on a Bruker SMART APEX II single crystal X-ray diffractometer with graphite-monochromated Mo K_α radiation ($\lambda = 0.71073 \text{ \AA}$) at room temperature. The obtained lattice parameters are $a = 0.8955(0.0019) \text{ nm}$, $b = 0.4153(0.0012) \text{ nm}$ and $c = 1.158(0.002) \text{ nm}$, which is consistent with the previous results.¹⁸ The directions of axis were also determined.

Electrical resistance measurements were performed using a four-probe configuration, with the applied current along the b -axis. Thin Pt wires were attached to electrical contacts made of epoxy. Electrical transport and heat capacity measurements were carried out in Quantum Design PPMS-9. The rotating sample holder was used to adjust the direction of the magnetic field. During the

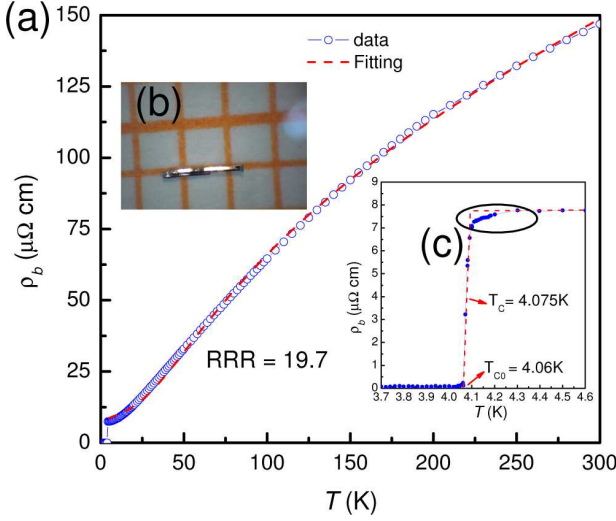


FIG. 1. (a) Temperature dependence of ρ_b (open circle) and its fitted curves (dashed line) for NiBi₃. (b) The photograph of single crystal of NiBi₃. (c) Temperature dependence of ρ_b for NiBi₃ vicinity the superconducting transition. The ellipse marks the initial resistivity drop.

MR measurements, H is perpendicular to the b - axis. Electron spin resonance (ESR) measurement was carried out in Bruker EMX-plus model spectrometer ($\nu \sim 9.4$ GHz).

III. RESULTS AND DISCUSSIONS

Figure 1(a) shows the temperature (T) dependence of resistivity along the b -axis (ρ_b) for NiBi₃ single crystal. Its superconducting transition can be seen in Fig. 1(c). The obtained T_{c0} is about 4.06 K, which is consistent with former results. The superconducting transition is sharp with a transition width $\Delta T_c \sim 0.04$ K. Interestingly, the $\rho_b - T$ curve has a initial drop around $T = 4.3$ K (Fig. 1(c)). Therefore, it rules out the possibility of the NiBi (S.G. $P6_3/mmc$, NiAs type) impurity with $T_c = 4.25$ K as the origin of the blunt specific heat (C) transition in the region from 4.1 K to 4.2 K in the polycrystalline sample.²¹ The residual resistivity ratio (RRR) is 19.7, higher than that of the polycrystalline sample.²¹ The initial drop is reminiscent of filamentary superconductivity that precedes bulk phase coherence, as observed in for example quasi-1D metal Nb₂Se₃.²² The ρ_b rises with positive curvature with increasing temperature below 22 K, and increases with a linear $\rho_b - T$ relation up to ~ 60 K. Then, ρ_b increases with a negative curvature above 60 K, and shows a saturation tendency towards high temperatures. The overall $\rho_b(T)$ follows the empirical model initially applied to A15 superconductors such as Nb₃Sn.²³ The model gives

$$\rho = \rho_0 + \rho_1 \cdot T + \rho_2 \cdot \exp\left(\frac{-T_0}{T}\right) \quad (1)$$

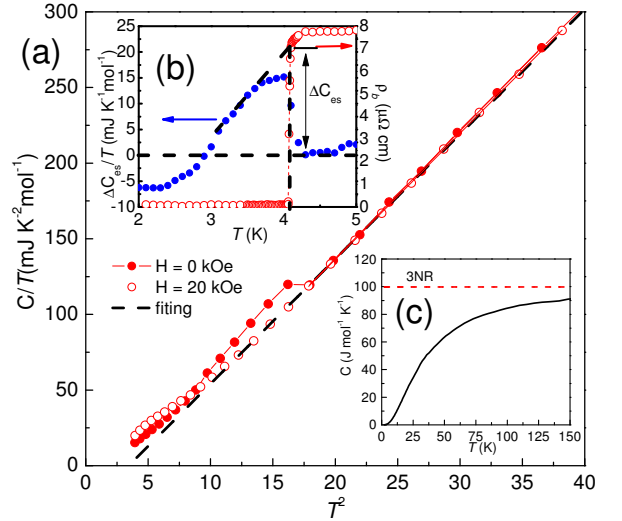


FIG. 2. (a) T^2 dependence of C/T of NiBi₃ for $H = 0$ kOe (solid circle) and $H = 20$ kOe (open circle); the linear fitting between 3 K and 6 K for $H = 20$ kOe. (b) The T dependence of $\Delta C_{es} = C(H = 0 \text{ kOe}) - C(H = 20 \text{ kOe})$ (Left panel) and the T dependence of ρ_b (right panel) for NiBi₃. (c) The T dependence of C for NiBi₃. The dashed line represents the 3NR, where N and R is the number of atoms in molecule and universal gas constant, respectively.

where, ρ_0 is the residual resistivity; ρ_1 , ρ_2 , and T_0 are material dependent parameters. The third term arises from the phonon-assisted scattering between the two Fermi-surface sheets. The fitted curve is shown in Fig. 1(a) as the dashed line. $\rho_0 = 7.453 \pm 0.016 \mu\Omega \cdot \text{cm}$, $\rho_1 = 0.244 \pm 0.004 \mu\Omega \cdot \text{cm K}^{-1}$, $\rho_2 = 96.2 \pm 1.5 \mu\Omega \cdot \text{cm}$, and $T_0 = 103.8 \pm 0.7$ K are determined from the fitted results. These values are comparable with those of Nb₃Sn.²³

Figure 2(a) shows the T^2 dependence of specific heat (C) divided by (T) of NiBi₃ single crystal for $H = 0$ kOe and $H = 20$ kOe. Obviously, no magnetic specific heat contribution can be observed. Around 4 K, a specific heat jump due to superconducting transition can be observed. The superconducting transition can be suppressed by $H = 20$ kOe. Interestingly, if we use the Sommerfeld - Debye expression $C = C_e + C_l = \gamma T + \beta T^3$ (γT is the electron contribution, and βT^3 is the lattice contribution) to fit the curve, the linear $C/T - T^2$ relation between 3 K and 6 K gives unphysical negative γ . This result is consistent with the previous reports.^{18,21} Yet, $\beta = 8.255 \pm 0.02 \text{ mJ mol}^{-1} \text{ K}^{-4}$ is obtained from the linear fitting between 3 K and 6 K. $\Theta_D = 98.0 \pm 0.1 \text{ K}$ can be estimated from the $\Theta_D = \sqrt[3]{12\pi^4 N R / 5\beta}$, where N is the number of atoms per molecule. In addition, the $C/T - T^2$ deviates from linearity below 3 K. Adding the anharmonic contribution $\sim T^5$ does not improve the fit. This is most likely due to the low Debye temperature ($\Theta_D \sim 100$ K).²¹ Most likely measurements of heat capacity below 2 K are necessary in order to reliably estimate γ . At high temperature, C for NiBi₃ approaches the ideal value of 3NR as the Dulong-Petit law predicts (Fig. 2(c)).

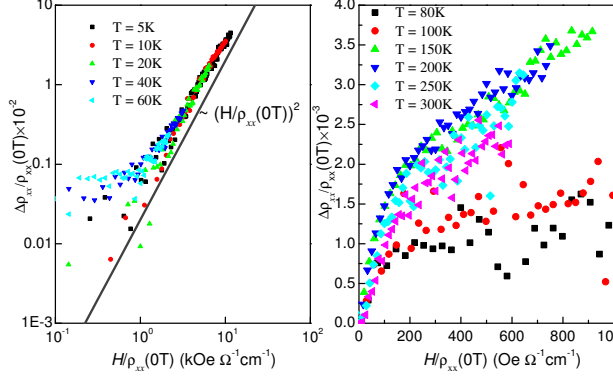


FIG. 3. (a) MR the Kohler's log-log plot in single crystals of for NiBi₃ at $T = 5, 10, 20, 40, 60$ K. (b) MR at different temperatures and the Kohler's plot in single crystals of for NiBi₃ at $T = 80, 100, 150, 200, 250, 300$ K.

In order to investigate the specific heat jump of superconducting transition, $C(H = 0 \text{ kOe}) - C(H = 20 \text{ kOe})$ is introduced to estimate the electronic specific heat in the superconducting state. Figure 2(b) shows the ΔC_{es} ($C(H = 0 \text{ kOe}) - C(H = 20 \text{ kOe})$) and $\rho_b - T$ curves. The $\Delta C_{es}/T \sim 20 \text{ mJ mol}^{-1} \text{ K}^{-2}$. From the McMillan formula

$$\lambda_{e-p} = \frac{\mu^* \ln(\frac{1.45T_c}{\Theta_D}) - 1.04}{1.04 + \ln(\frac{1.45T_c}{\Theta_D})(1 - 0.62\mu^*)}, \quad (2)$$

we estimate the electron-phonon coupling constant $\lambda_{e-p} \sim 0.91$ by assuming $\mu^* = 0.13$, which is a typical value for the Coulomb pseudo-potential.²⁶ This indicates that NiBi₃ is a strongly electron-phonon coupled superconductor.

Semiclassical transport theory predicts that Kohler's rule will be valid if there is a single species of charge carrier and the scattering time τ is the same at all points on the Fermi surface. MR at different temperatures can be scaled by the expression eq.(3) with the assumption that scattering rate $1/\tau$ is proportional to $\rho(T)$, and ω_c is the frequency at which the H causes the charge carriers to sweep across the Fermi surface:

$$\frac{\Delta\rho_{xx}(H, T)}{\rho_{xx}(0, T)} = f(\omega_c\tau) = f\left(\frac{H}{\rho(0, T)}\right), \quad (3)$$

and the corresponding plots are known as Kohler's plots.

Figure 3(a) depicts the Kohler's plot for NiBi₃ from 5 K to 60 K. Even at $H \perp b = 9 \text{ T}$, the MR is only about 4.5% at $T = 5 \text{ K}$. This value is very typical for a nonmagnetic metal. All curves collapse onto a single line, suggesting that the Kohler's rule is valid ($\Delta\rho_{xx}(H)/\rho_{xx}(0) \propto (\mu_0 H/\rho_{xx}(0))^2$). Figure 3(b) depicts the MR data $\Delta\rho_{xx}(H)/\rho_{xx}(0)$ as a function of $\mu_0 H/\rho_{xx}(0)$ above 80 K. Apparently, Kohler's rule is violated above 80 K. Due to the crystal structure, NiBi₃ should be a quasi-one dimensional system, whose Fermi surface topology is not

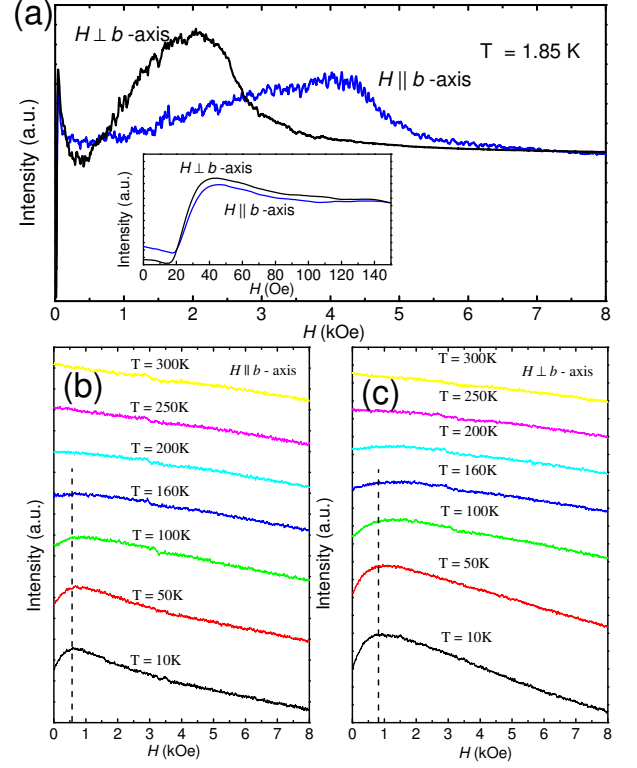


FIG. 4. (a) The ESR spectra of NiBi₃ measured at 1.85 K with sweeping H parallel to the b -axis and perpendicular to b -axis. Inset shows the amplified plots in the low field region. The ESR spectra of NiBi₃ measured at different temperatures with sweeping H parallel to the b -axis (b) and perpendicular to b -axis (c). The curves are shifted for clarity. The dashed lines mark the maximum of the ESR spectra.

spherical. The possible explanation is that multiband conductivity in NiBi₃. Below 60 K, the contribution of one band (with large $\omega_c\tau$) dominates whereas the contribution of other bands is negligible. The system can then be regarded as a single band conductor. Above 80 K the contributions are comparable, leading to deviation of the Kohler's rule. Similar phenomenon has been observed in low dimensional system, such as LiFeP.²⁷ What is important, the MR is positive below 300 K, indicating that NiBi₃ is not ferromagnetic in bulk.

Figure 4(a) shows the ESR (dP/dH) spectra of NiBi₃ measured at 1.85 K with sweeping H parallel to the b -axis ($H \parallel b$) and perpendicular to b -axis ($H \perp b$). Obviously, anisotropy can be observed. Both spectra show typical ESR signals for superconducting state. As shown in the inset, a stepwise sharp signal appears at low fields typical for the magnetic-shielding feature, indicating the appearance of superconductivity. Then, ESR signal show a hump below H_{c2} with increasing H .

Figure 4 (b) and (c) show the ESR spectra of NiBi₃ measured at different temperatures (above T_c) with sweeping $H \parallel b$ and $H \perp b$, respectively. No obvious resonance signal around $H = 3200 \text{ Oe}$ for paramagnetic

electron can be observed. Interestingly, the ESR spectra of NiBi₃ show abnormal diplike signal at low field below 160 K, which can be suppressed by increasing temperature. As marked by the dashed lines in Fig. 4 (b) and (c), the magnetic fields corresponding to diplike signal are anisotropic. In heavy fermion system CeRuPO, FM correlations is define by the ESR signal.²⁸ At low temperature below 10 K (Curie temperature = 15 K), ESR of CeRuPO shows similar diplike signals at low fields as well as NiBi₃. This diplike signal should be related to ferromagnetic moment fluctuations. At high temperature, the diplike signal of NiBi₃ disappears. The microwave signal of ESR can only exist on the surface of a metal (in μm length).²⁹ This strongly suggests that ferromagnetic moments fluctuations exist the surface on NiBi₃ below 160 K, and that NiBi₃ is non-magnetic in bulk. The crystal structure of NiBi₃ can be regarded as packing of NiBi₃ rods along the b - axis. In the bulk, the coordination of NiBi₃ rods has perfect translational symmetry; while on the surface, the translational symmetry is broken. The FM fluctuations in NiBi₃ could be attributed to the surface effect since surface tension modifies the electronic band structure, favoring FM on submicron length scale in nanostructured samples.¹⁵

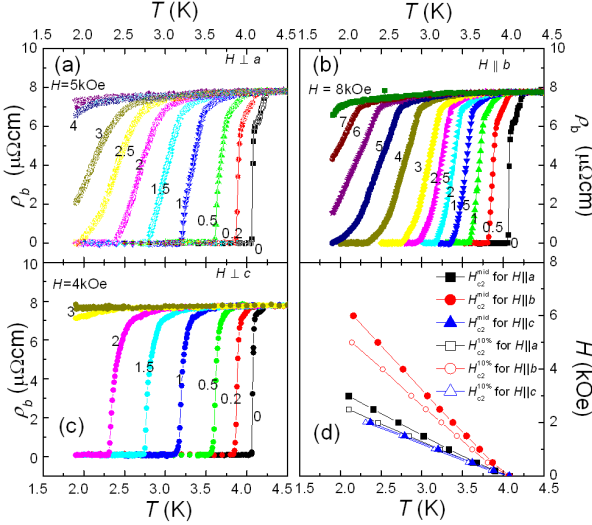


FIG. 5. Temperature dependence of the resistivity $\rho_b(T)$ of NiBi₃ for (a) $H \parallel a$, (b) $H \parallel b$ and (c) $H \parallel c$ at the various magnetic fields. (d) Temperature dependence of the upper critical field H_{c2} obtained from the midpoint and 10% on the $\rho_b - T$ curves for $H \parallel a$, $H \parallel b$ and $H \parallel c$.

Figure 5 (a), (b), and (c) show the $\rho_b - T$ curves at the various magnetic fields for $H \parallel a$, $H \parallel b$ and $H \parallel c$, respectively. The upper critical field (H_{c2}) is obtained from the midpoint and 10% resistivity on the $\rho_b - T$ curves, which is depicted in Fig. 5 (d). Obviously, H_{c2} show linear temperature dependence in the experimental temperature range. The obtained $[dH_{c2}^{mid}/dT]|_{T_c}$ ($[dH_{c2}^{10\%}/dT]|_{T_c}$) are 1.48(1.22), 3.13(2.60), and 1.17(1.14) kOe/K for $H \parallel a$, $H \parallel b$,

TABLE I. Parameters for NiBi₃.

T_{c0}	4.06 K				
ρ_0	$7.453 \pm 0.016 \mu\Omega \cdot \text{cm}$				
ρ_1	$0.244 \pm 0.004 \mu\Omega \cdot \text{cm} \text{ K}^{-1}$				
ρ_2	$96.2 \pm 1.5 \mu\Omega \cdot \text{cm}$				
T_0	$103.8 \pm 0.7 \text{ K}$				
ρ_{sat}	$328 \pm 2 \mu\Omega \text{ cm}$				
A_{ac}	$0.886 \pm 0.001 \mu\Omega \cdot \text{cm} \text{ K}^{-1}$				
λ_{e-p}	~ 0.91				
Θ_D	$98.0 \pm 0.1 \text{ K}$				
$H_c(0)$	$\sim 430 \text{ Oe}$				
		a	b	c	
$dH_{c2}/dT _{T_c}$	mid	1.48	3.13	1.17	kOe/K
	10%	1.22	2.60	1.14	kOe/K
$H_{c2}(0)$	mid	6.0	12.7	4.75	kOe
	10%	4.95	10.56	4.62	kOe
$H_{c1}(0)$	mid	65	41	75	Oe
	10%	71	47	74	Oe
$\xi(0)$	mid	18.1	38.3	14.3	nm
	10%	18.3	39.0	17.1	nm
$\kappa(0)$	mid	9.9	20.9	7.8	
	10%	8.14	17.4	7.6	
$\lambda_{GL}(0)$	mid	180	800	112	nm
	10%	149	678	130	nm
$m_a : m_b : m_c$	mid	4.48 : 1 : 7.15			
	10%	4.58 : 1 : 5.02			

and $H \parallel c$, respectively. According to the conventional one-band Werthamer-Helfand-Hohenberg (WHH) theory,³⁰ which describes the orbital limited H_{c2} of dirty type-II superconductors, $H_{c2} = 0.693[dH_{c2}/dT]|_{T_c}T_c$. Then $H_{c2}^a(0)$, $H_{c2}^b(0)$, $H_{c2}^c(0)$ can be obtained as 6(4.95), 12.7(10.56), and 4.75(4.62) kOe. The data in the brackets here and the following discussion are within the 10% resistivity results.

In the anisotropic superconducting system, coherence length (ξ_{GL}^i , where i is the axis) can be estimated from $H_{c2}^a = \frac{\Phi_0}{2\pi\xi_b\xi_c}$, $H_{c2}^b = \frac{\Phi_0}{2\pi\xi_a\xi_c}$, $H_{c2}^c = \frac{\Phi_0}{2\pi\xi_a\xi_b}$. The calculated ξ_{GL}^a , ξ_{GL}^b , ξ_{GL}^c are 18.1(18.3) nm, 38.3(39.0) nm, and 14.3(17.1) nm, respectively. The effective mass tensor is related to the GL coherence length as $m_a : m_b : m_c = 1/\xi_{GL}^a{}^2 : 1/\xi_{GL}^b{}^2 : 1/\xi_{GL}^c{}^2$. The calculated effective mass ratio $m_a : m_b : m_c$ 4.48:1:7.15(4.58:1:5.02). Obviously, NiBi₃ shows a quasi one dimensional behavior along the b - axis, with effective mass ratio $m_a^* \simeq m_c^*$ and $m_i^*/m_b^* \simeq 5$ (i represents a and c).

The thermodynamic critical magnetic field at $T = 0 \text{ K}$ ($H_c(0)$) can be estimated through $H_c(0) = [4\pi N(E_F)\Delta^2(0)]^{1/2}$. According to the band calculation, the density of states at Fermi surface $N(E_F)$ is 2.55 states/eV f.u.¹⁸ By assuming the $\Delta(0) = 1.76k_B T_c$, H_c is estimated to be $\sim 430 \text{ Oe}$. This value is consistent with experimental results.¹⁸ GL parameter κ , the lower critical field at zero temperature ($H_{c1}(0)$), and the penetration depth λ_{GL} at $T = 0 \text{ K}$ can be estimated from: $H_{c2}^i = \sqrt{2}\kappa^i H_{c1}^i$, $H_{c1}^i = H_c \frac{\ln \kappa^i - 0.18}{\sqrt{2}\kappa^i}$, and $\lambda_{GL}^i = \kappa^i \xi_{GL}^i$, where i represents the direction of a, b, c . The estimated

parameters in the superconducting state and the parameters in the normal state mentioned above are listed in Tab. I.

IV. SUMMARY

We investigated anisotropy in superconducting and normal state properties of NiBi₃. The carrier scattering mechanism is dominated by electron-phonon scattering whereas MR suggests the absence of magnetic scattering commonly observed in bulk FM materials. The heat capacity results indicates it is a strongly $e - p$ coupling superconductor. However, FM fluctuations are detected at the surface of the crystal. Finally, we give anisotropic

superconducting parameters.

V. ACKNOWLEDGEMENT

We thank Dr. Wei Tong for the help on ESR measurements. Work at Brookhaven National Laboratory (H. L. and C. P.) was supported by the US DOE under Contract No. DE-AC02-98CH10886. Work at High magnetic field lab (Hefei) was supported by the State Key Project of Fundamental Research, China (2010CB923403) and National Basic Research Program of China (973 Program), No. 2011CBA00111.

* Email:xdzhu@hmfl.ac.cn

-
- ¹ D. Fay and J. Appel, Phys. Rev. B **22**, 3173 (1980).
 - ² S. S. Saxena, P. Agarwal, K. Ahilan, F. M. Grosche, R. K. W. Haselwimmer, M. J. Steiner, E. Pugh, I. R. Walker, S. R. Julian, P. Monthoux, G. G. Lonzarich, A. Huxley, I. Sheikin, D. Braithwaite, and J. Flouquet, Nature **406**, 587 (2000).
 - ³ D. Aoki, A. Huxley, E. Ressouche, D. Braithwaite, J. Flouquet, J.-P. Brison, E. Lhotel, and C. Paulsen, Nature **413**, 613 (2001).
 - ⁴ N. T. Huy, A. Gasparini, D. E. de Nijs, Y. Huang, J. C. P. Klaasse, T. Gortenmulder, A. de Visser, A. Hamann, T. Gorlach, and H. v. Lohneysen, Phys. Rev. Lett. **99**, 067006 (2007).
 - ⁵ C. Pfleiderer, M. Uhlarz, S. M. Hayden, R. Vollmer, H. v. Löhneysen, N. R. Bernhoeft, and G. G. Lonzarich, Nature **412**, 58 (2011).
 - ⁶ E. A. Yelland, S. M. Hayden, S. J. C. Yates, C. Pfleiderer, M. Uhlarz, R. Vollmer, H. v. Löhneysen, N. R. Bernhoeft, R. P. Smith, and S. S. Saxena, Phys. Rev. B **72**, 214523 (2005).
 - ⁷ G. M. Schmiedeshoff, C. DeBoer, M. V. Tompkins, W. P. Beyermann, A. H. Lacerda, J. L. Smith, and P. C. Canfield, J. Supercond. Novel Magnet. **13**, 847 (2000).
 - ⁸ M. Kenzelmann, Th. Strässle, C. Niedermayer, M. Sigrist, B. Padmanabhan, M. Zolliker, A. D. Bianchi, R. Movshovich, E. D. Bauer, J. L. Sarrao, and J. D. Thompson, Science **321**, 1652 (2008).
 - ⁹ E. Blackburn, P. Das, M. R. Eskildsen, E. M. Forgan, M. Laver, C. Niedermayer, C. Petrovic, and J. S. White, Phys. Rev. Lett. **105**, 187001 (2010).
 - ¹⁰ J. W. Lynn, G. Shirane, W. Thomlinson, and K. N. Shelton, Phys. Rev. Lett. **46**, 368 (1981).
 - ¹¹ A. Ahmed, M. Itou, S. Xu, Z. Xu, G. Cao, Y. Sakurai, J. Penner-Hahn, and A. Deb, Phys. Rev. Lett. **105**, 207003 (2010).
 - ¹² D. E. Moncton, D. B. McWhan, P. H. Schmidt, G. Shirane, W. Thomlinson, M. B. Maple, H. B. MacKay, L. D. Woolf, Z. Fisk, and D. C. Johnston, Phys. Rev. Lett. **45**, 2060 (1980).
 - ¹³ H. Mizoguchi, S. Matsuishi, M. Hirano, M. Tachibana, E. Takayama-Muromachi, H. Kawaji, and H. Hosono, Phys. Rev. Lett. **106**, 057002 (2011).
 - ¹⁴ E. L. Martinez Piñeiro, B. L. R. Herrera, and R. Escudero, Solid State Commun. **151**, 425 (2011).
 - ¹⁵ T. Herrmannsdörfer, R. Skrotzki, J. Wosnitza, D. Köhler, R. Boldt, and M. Ruck, Phys. Rev. B **83**, 140501(R) (2011).
 - ¹⁶ M. Sakurai, T. Ono, I. Yoshida, and S. Tanuma, Jpn. J. Appl. Phys. **39**, 6366 (2000).
 - ¹⁷ B. Jayaram, S. N. Ekbote, and A. V. Narlikar, Phys. Rev. B **36**, 1996 (1987).
 - ¹⁸ J. Kumar, A. Kumar, A. Vajpayee, B. Gahtori, D. Sharma, P. K. Ahluwalia, S. Auluck, and V. P. S. Awana, Supercond. Sci. Technol. **24**, 085002 (2011).
 - ¹⁹ H. Yoshida, T. Shima, T. Takahashi, T. Kaneko, T. Suzuki, H. M. Kimura, K. Asami, and A. Inoue, J. Magnet. Magnet. Mater. **239**, 5 (2002).
 - ²⁰ P. C. Canfield and Z. Fisk, Phil. Mag. B **65**, 1117 (1992).
 - ²¹ Y. Fujimori, S.-i. Kan, B. Shinozaki, and T. Kawaguti, J. Phys. Soc. Jpn. **69**, 3017 (2000).
 - ²² R. Hu, K. Lauritsch-Kullas, J. O'Brian, V. F. Mitrovic, and C. Petrovic, Phys. Rev. B **75**, 064517 (2007).
 - ²³ D. W. Woodward and G. D. Cody, Phys. Rev. **136**, A166 (1964).
 - ²⁴ M. Gurvitch, Phys. Rev. B **24**, 7404 (1981).
 - ²⁵ D. Varshney and N. Kaurav, Eur. Phys. J. B **40**, 129 (2004).
 - ²⁶ S. B. Dugdale, Phys. Rev. B **83**, 012502 (2011).
 - ²⁷ S. Kasahara, K. Hashimoto, H. Ikeda, T. Terashima, Y. Matsuda, and T. Shibauchi, Phys. Rev. B **85**, 060503(R) (2012).
 - ²⁸ C. Krellner, T. Förster, H. Jeevan, C. Geibel, and J. Sichelschmidt, Phys. Rev. Lett. **100**, 066401 (2008).
 - ²⁹ Skin effect depth $= \sqrt{\rho/\pi f \mu}$, where ρ is the resistivity of the conductor in m , f is frequency in Hertz, and μ is the absolute magnetic permeability of the conductor. The absolute magnetic permeability $\mu = \mu_0 \cdot \mu_r$, where $\mu = 4\pi \times 10^{-7}$ H/m, and μ_r is the relative magnetic permeability. Since NiBi₃ is not magnetic in bulk, here we use $\mu_r = 1$ to estimate the Skin effect depth. As for NiBi₃, $f = 9.4$ GHz, $\rho = 8 - 150 \times 10^{-8}$ ohm m. The skin depth should be 1.5 - 6.4 μ m.
 - ³⁰ N. R. Werthamer, E. Helfand, and P. C. Hohenberg, Phys. Rev. **147**, 295 (1966).